WILEY | Hindawi

Research Article

Inertial Gyro Wave Energy Conversion Nonlinear Modeling and Power-Index Predictive Control for Autonomous Ship

Nailong Wu [iD],[1] **Xinyuan Chen** [iD],[1] **Shaonan Chen,**[2] **Haodong Yuan** [iD],[1] **Jie Qi** [iD],[1] **and Yueying Wang** [iD][3]

[1]*College of Information Science and Technology, Donghua University, Shanghai 201620, China*
[2]*Shanghai Jiwu Technology Co., Ltd., Shanghai 201612, China*
[3]*School of Mechatronic Engineering and Automation, Shanghai University, Shanghai 200444, China*

Correspondence should be addressed to Haodong Yuan; hdyuan@dhu.edu.cn

The complex marine environment and the high energy consumption of shipboard equipment pose challenges to the long-term navigation of autonomous unmanned ships. In wave-induced motion, inertial gyro antirolling technology is used to offset the energy transmitted by waves, but the massive consumption of energy is not conducive to long-term navigation of the unmanned ships. This paper attempts to exploit the wave energy transmitted by the gyro to improve the power supply of the unmanned ship. Firstly, a nonlinear coupling model of the gyro antirolling device and the unmanned ship is established. Secondly, considering various model constraints and physical constraints of the equipment, the energy evaluation objective function of nonlinear model predictive control (NMPC) is designed. In the simulation, the proposed control method can effectively extract electric energy from different waves.

1. Introduction

The control of Unmanned Surface Vehicle (USV) is challenging due to the unpredictable disturbances from the complex ocean environment, the model uncertainties, and the signal tremor caused by the controller [1–3]. Among them, the wave disturbance exerted on the unmanned vehicle during the navigation should be paid more attention [4–7]. In order to reduce the influence of waves on the rolling motion of the ship when it is stationary or sailing in the ocean, gyro antirolling technology has become a feasible solution. However, the gyro equipment is mainly supported by the onboard energy system rather than the energy obtained from the ocean [8–10].

With the purpose of extracting energy from the ocean effectively, some researchers focus on the power generation control of inertial sea wave energy converter (ISWEC) [11–14]. For example, Raffero et al. analyzed the influence of the damping of the power take-off (PTO) shaft on the gyroscope and improved the control performance by considering the maximum constraint of PTO torque [15]. Vissio et al. proposed linear quadratic regulator (LQR) to optimize the energy production efficiency of ISWEC device [16]. Bracco et al. introduced the model prediction method into the optimal control of the mooring power generation [17–19]. However, the above research is implemented based on the nominal linear model, and the nonlinear term and the mismatch caused by the time-varying evolution of the model are ignored. Since the controller is developed via treating the linear system as the reference model, it is difficult to overcome the actual wave excitation. In order to study the influence of the nonlinear characteristics on the wave energy converter (WEC), Richter et al. and Mérigaud and Ringwood have exploited the nonlinear represented model of the WEC [20, 21]. Nonetheless, the authors pay more attention to the power generation of WEC in mooring state.

The inertial sea wave energy converter can be incorporated into the floating mooring platform; thus it can provide electrical energy for the wave power stations on the coast. At present, the energy onboard limits the range of the

unmanned ship. When the electricity extracted by the inertial wave energy converter is integrated into the power management system of unmanned ship, a new hybrid power supply system of the unmanned ship can be established. It can enhance the endurance and the ocean energy utilization of unmanned ships effectively.

In the research of Bracco et al., the device's hull is retained by a slack mooring. Thus, it is capable of adjusting the attitude relative to the waves itself, and the system can extract energy from the wave via pitching the floating vessel back and forth. Whereas the unmanned ship with ISWEC device is sailing in the ocean rather than in a fixed anchored state, the vessel model characteristics are different. On the one hand, unmanned ships are capable of navigating and tracking desired path in the ocean. ISWEC equipment is expected to occupy less space and have low energy consumption. On the other hand, it is not necessary to consider the limitation on the pitch angle of the hull in the mooring floating body. However, the excessive roll angle will affect the navigation safety of the ship. The unique dynamic characteristics of sailing ships bring about more challenges to the design of controllers.

From the perspective of the energy transfer, the gyro stabilizer is a machine that can convert the ocean wave energy to the mechanical kinetic energy of the gyro precession motion. When the ship navigates in the adverse ocean situations, the vessel tends to shake around the boat roll axis due to the fluctuating waves on the surface [22]. The rolling motion of the ship is accompanied by the rotation motion of the flywheel rotor to produce a gyro effect, which generates a torque on the precession axis of the gyro stabilizer. While a PTO is connected to the precession axis as a damper, the torque on the precession axis can be used to drive the electrical generator [23, 24]. The advantage utilizing the gyroscopic system is that the equipment is completely enclosed, and the mechanical parts are not exposed to the harsh marine environment. The wave energy can be extracted via ISWEC with high reliability and safety [25]. Considering the strong coupling between the ship and the ISWEC system, it is not convenient to decouple the equation completely; and the uncertainty of model parameters and external nonlinear disturbance play a great impact on the control performance [26]. To address this problem, the designed controller is expected to deal with the time-varying wave excitation in a predictive way [27–30].

Compared with the linear quadratic regulator optimization method, MPC method can improve the power generation of the wave energy converter significantly while meeting the control torque and precession constraints [31–34]. The predictive control can take into account the future state and the output of the system, and the multistep iterative predictive model is adopted to construct the objective function. It not only pays more attention to the nonlinear characteristics of the system but also considers various constraints in the actual control [35, 36]. Aiming at optimizing the power generation in ISWEC system, the overall performance index of the control can be reflected by introducing the cost function. The physical constraint of the system is defined in terms of mechanical characteristics. The

nonlinear model predictive control method has been successfully applied to the optimal estimation of lithium-ion batteries, the safe fatigue design of wind turbines, and the fast response of turboshaft engines [37–39].

In this paper, the motivation is to study the gyro wave power generation to improve the ship energy supply; NMPC method is introduced to cope with the power generation problem of the coupling dynamic system including the ship, gyroscope, and PTO. The limitations of the PTO torque, precession angle, and precession angular velocity are key factors in the actual system. In the existing research, the mathematical model of gyro wave energy converter is mostly based on the linear model of a ship. In this paper, a nonlinear rolling model is derived to decrease the minimum deviation between the predicted output of the controller and the actual result as soon as possible. The effect of the error can be improved via adding appropriate constraints. The CasADi solver is employed to obtain the results of the nonlinear optimization problem online [40]. Numerous simulation tests are carried out to verify the feasibility of the control strategy, and the power generation of shipboard ISWEC with different control methods is compared and analyzed.

The remaining parts of the paper are organized as follows. In Section 2, the dynamic models for each part of the power generation system of ISWEC are described and the dynamic model of the whole system is established. In Section 3, NMPC control method is introduced, and the specific control scheme for NMPC framework is designed. In Section 4, the simulation results and discussions are presented to assess the effectiveness of the proposed method. Finally, the conclusion is given in Section 5.

2. System Model

2.1. Wave Excitation Model. To study the power generation performance of the ISWEC mechanism amounted on an autonomous ship, it is firstly necessary to establish a suitable wave excitation model to simulate the actual hydrological conditions. There are two types of waves generally: the regular wave and the random wave. The regular wave can be described by the wave height H and the wave period T. The regular wave is shaped like a sine curve, which can be depicted by the following formula:

$$z(t) = \frac{H}{2}\sin(\omega t), \tag{1}$$

where z is the wave height relative to the still water level and the angular frequency $\omega = 2\pi/T$ defines the periodicity of the wave in time.

The random wave models can be divided into the two-dimensional random sea wave model with long-crested waves and the three-dimensional random sea wave model with irregular short-crested waves. The long-crested waves refer to waves propagating in a certain direction. The crests and valleys are parallel to each other and perpendicular to the forward direction of the wave. The short-crested waves are generated by the wind excitation. Due to the randomness of the wind direction, the waves propagate in all directions randomly. In this paper, two-dimensional irregular long-

crested wave is used as the random wave excitation to study the dynamic characteristics of the ship.

The moment exerted on the ship by ocean waves is the function of the wave surface slope. To describe the slope of wave surface model of random waves, the wave spectrum should be acquired. The commonly used ocean wave spectrum includes Pierson–Moskowitz spectrum (PM spectrum), ITTC dual parameter spectrum (ISSC spectrum), and AK Fung spectrum. Since the PM spectrum is suitable for the infinite water depth, it has been widely used in the fields of ocean engineering and ship engineering. In this article, the PM spectrum corrected in 1969 is selected as the simulated spectrum [41], and it can be listed as follows:

$$s(\omega) = \frac{173 H_s^2}{\omega^5 T_s^4} \exp\left(\frac{-691}{\omega^4 T_s^4}\right), \qquad (2)$$

where H_s is the significant wave height and T_s is the average period. According to the wave spectrum function $s(\omega)$, the spectrum function of the the wave surface slope $\zeta(\omega)$ can be obtained as follows:

$$\zeta(\omega) = \frac{\omega^4}{g^2} s(\omega), \qquad (3)$$

where g is the gravitational acceleration. The slope function of wave surface can be regarded as a zero-mean stationary random process, and it is obtained via transforming the frequency domain expression of the wave surface slope into the time domain expression; thus the slope of wave surface at a fixed point in the sea wave can be defined as shown below:

$$\zeta_\alpha(t) = \left[\sum_{n=1}^{N} \sqrt{2 \int_{\omega_{n-1}}^{\omega_n} \zeta(\omega) d\omega} \, \cos\left(\omega_r t + \varepsilon_n\right)\right] \sin(\psi), \qquad (4)$$

where ω is the harmonic angular frequency, ε_n indicates the uniformly distributed random phase angle within $(0, 2\pi)$, and N reflects the number of harmonics to be selected. The encounter angular frequency can be obtained from the equation $\omega_r = \omega - kv \cos(\psi)$, where k is the wave number, v is the speed of the ship, and ψ denotes the heading angle.

2.2. Nonlinear Dynamic Model. Autonomous ships moving on the water surface produce various oscillatory motions due to the interference of sea waves [22, 42]. Because the damping in the roll channel is expected to be very small, it brings about larger amplitude oscillations to the vessel. The power generation efficiency of the device can be improved by the help of ISWEC technique. The incident wave is regarded as a two-dimensional long-crested ocean wave, and the coupling effect of the ship motion in different degrees of freedom is neglected. In this paper, the interaction between the incident wave and the equipment is investigated on the plane defined by the vertical axis of the hull and the horizontal axis of the hull [43].

According to the dynamic balance theory, the dynamic equation of the autonomous ship in the roll channel can be given as follows:

$$(I_\delta + \triangle I_\delta)\ddot{\delta} + A(\dot{\delta}, t) + B(\delta, t) = M_w(\psi, \omega_r, t), \qquad (5)$$

where δ is the roll angle of the ship, I_δ is the inertia moment of the hull, ΔI_δ is the additional inertia moment of the hull, and the sum of I_δ and ΔI_δ indicates the total inertia moment of the hull. Additionally, $A(\dot{\delta}, t)$ is the roll damping moment, $B(\delta, t)$ defines the roll restoring moment, $M_w(\psi, \omega_r, t)$ describes the wave excitation moment, and ω_r is the encounter angle frequency.

When the roll angle is small (generally within $\pm 8°$), the linear form is selected to describe the roll damping moment of the ship. However, the linear form of the damping moment brings about more errors to the calculation when the roll angle is too large. Therefore, it is necessary to determine the rigor of this treatment when choosing the nonlinear form of the damping moment to replace the linear form. At present, the first common nonlinear form of the damping moment equals the sum of the linear damping and the square damping [44]. Besides, the damping moment can be obtained from the sum of the linear damping and cubic damping [45, 46]. In this paper, the latter damping moment expression is chosen:

$$A(\dot{\delta}, t) = A_1 \dot{\delta} + A_3 \dot{\delta}^3, \qquad (6)$$

where the damping coefficient is directly obtained from the ship parameter table in this paper.

The restoring moment is affected by the roll, pitch, and heave of the ship; thus the modeling for the moment is difficult. Since only the roll degree of freedom is considered in this paper, other channels of the ship are ignored in this paper [43]. The stability height of the ship is time-invariant, so the restoring moment can be expressed as

$$B(\delta, t) = B_1 \delta + B_3 \delta^3 + B_5 \delta^5, \qquad (7)$$

where the restoring moment coefficients B_1, B_3, and B_5 are obtained from the ship parameter table.

The wave excitation moment can be expressed as a function of the wave surface slope as follows:

$$M_w(t) = M_D h_{GM} \zeta_\alpha(t), \qquad (8)$$

where M_D is the displacement of the ship, h_{GM} is transverse metacentric height, and $\zeta_\alpha(t)$ is the slope of the wave surface. Based on the above discussions, substituting the above equation into equation (5), the nonlinear rolling dynamic equation of the ship excited by waves can be obtained as follows:

$$\ddot{\delta} = \frac{-a_1 \dot{\delta} - a_3 \dot{\delta}^3 - b_1 \delta - b_3 \delta^3 - b_5 \delta^5 + M_D h_{GM} \zeta_\alpha(t)}{(I_\delta + \triangle I_\delta)}, \qquad (9)$$

where $a_i = A_i/(I_\delta + \triangle I_\delta)$, $(i = 1, 3)$; $b_i = B_i/(I_\delta + \Delta I_\delta)$, $(i = 1, 3, 5)$.

The power generation principle of the ISWEC equipment is as follows: the waves acting on the hull make the ship roll around x-axis of the vessel frame, and the energy is transmitted to the gyroscopic system inside the boat. The gyroscopic system is amounted on the center of the boat, and the main part is the flywheel that can rotate around a vertical

axis at high speed. When the gyroscopic system is working, the gyro effect is the result of the flywheel rotation speed w_0 and the ship roll speed $\dot{\delta}$, which generates a torque M in the precession axis. The torque is then transmitted to a rotary driven power generator. The power generated can be integrated into the power supply for the ship.

The coordinate system is shown in Figure 1. Firstly, the base coordinate system $O - x'y'z'$ of the gyroscopic device is given, where O is the fixed connection point between the ship and the gyroscopic system, the $O - x'$ axis points to the bow, the $O - y'$ axis points to the port side of the ship, and the $O - z'$ axis points to the vertical direction of hull deck. The roll angle of the hull around the longitudinal axis $O - x'$ is δ. The $O - xyz$ frame coordinate system can be regarded as a rotating coordinate system relative to $O - x'y'z'$, where the Oz axis is the flywheel rotation axis of the rotor and the Oy axis is the gyro precession axis. Regardless of the motion influence of the ship on the gyro antirolling device's other degrees of freedom, the high-order terms in the equation are omitted. Therefore, the motion equation of the antirolling gyro relative to the rotating coordinate system $O - xyz$ can be established according to the Newton balance method:

$$M_x = J\ddot{\delta}\cos\varepsilon + h_0\dot{\varepsilon},$$
$$M_y = J\ddot{\varepsilon} + J\dot{\delta}^2\sin\varepsilon\cos\varepsilon - h_0\dot{\delta}\cos\varepsilon, \quad (10)$$
$$M_z = I\dot{\omega}_0 = 0,$$

where I is the inertia moment of the flywheel rotor relative to the Oz axis, J represents the inertia moment of the rotor relative to the Ox and Oy axes, the rotor speed is constant with the value w_0, and ε defines the precession angle of the rotor around the Oy axis. M_x, M_y, and M_z are the components of the external moment M in each direction of the $O - xyz$ frame coordinate system, respectively. $h_0 = Iw_0$ indicates the momentum constant of the antirolling gyroscope. The Oy axis is regarded as the output axis and the moment of gyroscope subjected to the damper is M_y; thus the plant output torque M_y is obtained from the Oy axis. The output torque in the $O - xyz$ coordinate system is then represented in the translational coordinate system $O - x'y'z'$. Due to the gyro effect of the high-speed rotating flywheel, the angular velocities $\dot{\delta}$ along with $\dot{\varepsilon}$ are extremely small compared with w_0, so the second-order term is ignored. Equation (10) can be simplified:

$$M_{x'} = h_0\dot{\varepsilon}\cos\varepsilon,$$
$$M_{y'} = M_y = J\ddot{\varepsilon} - h_0\dot{\delta}\cos\varepsilon, \quad (11)$$
$$M_{z'} = h_0\dot{\varepsilon}\sin\varepsilon.$$

It can be seen from the above formula that the gyro effect not only produces torque in the direction of the precession axis Oy but also brings about similar torque to the Ox and Oz axes. On the Ox axis, the moment caused by the angular velocity w_0 and ε is always opposite to the rolling direction, which is generally used to counteract the ship rolling motion induced by the sea wave. That is why the gyroscopic

stabilizer can reduce the ship rolling. On the Oz axis, the interference torque generated by the angular velocity w_0 and ε can increase the oscillation of the ship in the yaw channel. However, when a pair of gyroscopic stabilizers with the opposite rotation direction and same rotation speed are amounted in the vessel, the disturbance moment in the yaw direction of the boat introduced by the gyroscopic system can be improved. In the process of modeling the ISWEC power generation device for an autonomous ship, the dynamic models of multiple gyroscopic devices can be equivalent to a single gyro dynamic model.

In the previous part of this paper, the wave excitation model, ship roll dynamics model, and gyro device model are listed. The previously mentioned models can be combined to obtain a joint dynamics model of the entire system as follows:

$$\ddot{\delta} = -a_1\dot{\delta} - a_3\dot{\delta}^3 - b_1\delta - b_3\delta^3 - b_5\delta^5$$
$$+ \frac{M_D h_{GM}\zeta_\alpha(t)}{I_\delta + \Delta I_\delta} - \frac{2nh_0\dot{\varepsilon}\cos\varepsilon}{I_\delta + \Delta I_\delta}, \quad (12)$$
$$\ddot{\varepsilon} = \frac{h_0\dot{\delta}\cos\varepsilon}{J} - \frac{M}{J},$$

where M is the damping torque of the PTO.

In the mentioned model above, when the singular output of the gyroscopic device occurs, the precession angle of the gyroscopic system remains at $90°$ or $-90°$ Meanwhile, the precession of the gyroscopic equipment cannot rotate around the precession axis, and finally the device loses its power generation capability. In order to avoid the singular output of the gyroscopic device, the center of gravity of the device should be lower to obtain the gravitational restoring torque. The joint dynamic model can be given:

$$\ddot{\delta} = -a_1\dot{\delta} - a_3\dot{\delta}^3 - b_1\delta - b_3\delta^3 - b_5\delta^5$$
$$+ \frac{M_D h_{GM}\zeta_\alpha(t)}{I_\delta + \Delta I_\delta} - \frac{2nh_0\dot{\varepsilon}\cos\varepsilon}{I_\delta + \Delta I_\delta}, \quad (13)$$
$$\ddot{\varepsilon} = \frac{h_0\dot{\delta}\cos\varepsilon}{J} - \frac{M}{J} - \frac{x_{\text{offset}}M_G\sin\varepsilon}{J},$$

where x_{offset} is the distance from the center of gravity of the gyroscope to the precession axis, M_G is the gyro mass, and $2n$ is the gyro number.

2.3. Linear Dynamic Model.

The system motion is described by a nonlinear and coupled equation. In order to evaluate the dynamic characteristics of the system, the equation should be resolved numerically. The nonlinear system is simplified to a linearized equation at the equilibrium point. The linearization approximation is carried out at the steady-state point of the system $\varepsilon = 0$. The following formula gives the linear form of the gyroscopic dynamic equation:
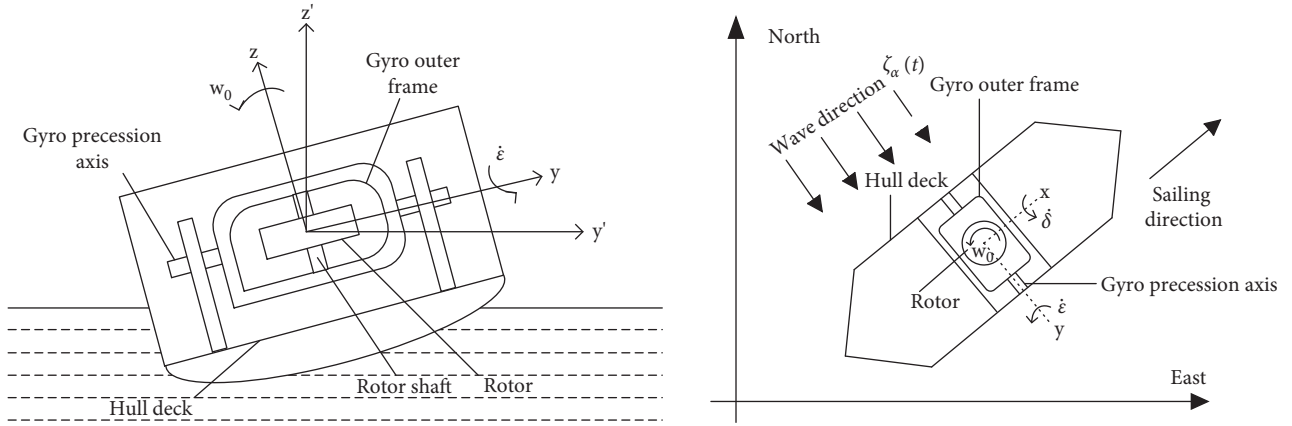
FIGURE 1: The coordinate system of dynamic model.

$$M_{x'} = h_0\dot{\varepsilon},$$
$$M_{y'} = M_y = J\ddot{\varepsilon} - h_0\dot{\delta}, \quad (14)$$
$$M_{z'} = h_0\dot{\varepsilon}\varepsilon.$$

In the previous part, the linear damping plus cubic damping proposed by Froude is composed to determine the damping moment of a ship in the roll channel. The polynomial form is used to approximate the restoring moment of the ship. However, when the rolling angle of the ship is small, the damping moment and restoring moment of the ship can be expressed in the linear form, and only the first-order term in the original polynomial is retained [41]. Thus, the simplified rolling dynamics equation is given:

$$\ddot{\delta} = \frac{-a_1\dot{\delta} - b_1\delta + M_D h_{GM}\zeta_\alpha(t)}{(I_\delta + \Delta I_\delta)}. \quad (15)$$

Therefore, the joint linear dynamic model of the system can be obtained by replacing the original nonlinear model with the linearized ship roll model and the gyroscopic model:

$$\ddot{\delta} = -a_1\dot{\delta} - b_1\delta + \frac{M_D h_{GM}\zeta_\alpha(t)}{I_\delta + \Delta I_\delta} - \frac{2nh_0\dot{\varepsilon}}{I_\delta + \Delta I_\delta},$$
$$\ddot{\varepsilon} = \frac{h_0\dot{\delta}}{J} - \frac{M}{J} - \frac{x_{\text{offset}}M_G\varepsilon}{J}. \quad (16)$$

3. Control Scheme

3.1. NMPC Method.
ISWEC power generation can be controlled by the passive control and the active control approach. When designing the passive controller, the impact of changes in the main parameters of the system on the absorbed power should be analyzed. Then the best parameters of the power generation power equipment under specific hydrological conditions can be determined. Thus, the maximum power generation can be guaranteed. Moreover, the system control parameters remain unchanged during the entire power generation process. The advantage of the passive control is that the parameters are only

determined once and the method is simple. However, the boat sails at a changeable hydrological environment, and the passive control system cannot update the parameters in real time, which can only ensure that the determined parameters are the optimal values in the statistical view. The power generation efficiency at each step is not optimized actually. Therefore, many controllers with real-time control capabilities are introduced into the power generation control of ISWEC equipment, which is a kind of active control for power generation equipment. Among them, model predictive control has gained more and more attention in utilization of ocean energy because of its predictive ability and the capability to handle multiple performance indicators and multiple constraints effectively.

The model predictive control method mainly includes three steps: predicting the future state based on the model, solving the optimization problem using the numerical method, and applying the first component of the optimal control sequence to the system. The characteristics of MPC, such as real-time update, rolling optimization, and model prediction, make MPC controller have more robustness, and it still maintains better control performance in the case of the high uncertainty of the controlled object itself and the external disturbance brought by the wave.

3.2. Controller Design.
In ISWEC, the electrical energy comes from the precession motion of the gyro device. The precession motion is generated by the gyroscopic effect that is produced by the rolling motion caused by the wave and the rotation of the flywheel. Hence, the power generated by the ISWEC device on the precession shaft equals the product of the precession angular velocity and the damping torque; namely,

$$P_{\text{PTO}} = \dot{\varepsilon}M. \quad (17)$$

The effective control of the power generation is realized by adjusting the damping torque of PTO. The above formula describes the relationship between the overall controlled object and the control input, and it can be seen that the system optimizes the power generation by adjusting the PTO damping torque. Power is the principal index of

optimization. The relationship of the energy transfer and conversion in ISWEC system is shown in Figure 2.

In order to optimize the energy conversion, the power should be maximized in the control design program. M applied to the precession axis by the PTO is also the control input. In order to optimize the energy generation, the control torque must be minimized. Thus, the control input should be treated as a control indicator of the cost function. Furthermore, the importance of the two indicators can be traded off by the weighting coefficients. The state variables are as follows:

$$x(t) = \begin{bmatrix} x_1 & x_2 & x_3 & x_4 \end{bmatrix}^T = \begin{bmatrix} \delta(t) & \dot{\delta}(t) & \varepsilon(t) & \dot{\varepsilon}(t) \end{bmatrix}^T \in \mathbb{R}^4. \tag{18}$$

Thus, the cost function of the NMPC method can be expressed as follows:

$$\min_M J(t) = \sum_{i=0}^{N_p-1} x^T(t+i)PM(t+i) + \sum_{i=0}^{N_c-1} M^T(t+i)RM(t+i), \tag{19}$$

where P and R are the weighting matrices.

The cost function of the LQR method can be expressed as follows:

$$\min_M J = \int_{t_o}^{t_f} x^T(t)Qx(t) + x^T(t)NM(t) + r_T M^2(t)dt, \tag{20}$$

where Q, N, and r_T are the weighting matrices.

There are generally two types of controller constraints when designing the model predictive controller. The first one

is the dynamic constraints. In the above-mentioned joint dynamics model, the design of the controller should consider the electrical and mechanical constraints of the actual system. The precession angle and the angular velocity of precession must conform to the requirements of the physical constraints and the predetermined area cannot be exceeded. The other constraint is the range restriction of the control variables. The opening and closing of the valve are limited and the control variables of the system are not allowed to exceed the mechanical constraints of the valve. Therefore, all of the constraints including the precession angle, precession angular velocity, and the control output range of the ISWEC device should be adjusted reasonably. At time k, when the prediction range is N_p and the control range is N_c, the precession angle, precession angular velocity, and the control output range of the system can be confirmed, which can be expressed as follows:

$$|M(k+i|k)| \le M_{max}, \quad i = 0,\ldots,N_c-1,$$
$$|\varepsilon(k+i|k)| \le \varepsilon_{max}, \quad i = 0,\ldots,N_p-1, \tag{21}$$
$$|\dot{\varepsilon}(k+i|k)| \le \dot{\varepsilon}_{max}, \quad i = 0,\ldots,N_p-1,$$

where M_{max} is the constraint of the control quantity, while ε_{max} and $\dot{\varepsilon}_{max}$ are the state constraints. It should be noted that $N_c \le N_p$.

Since a discrete time model should be provided for the MPC controller, the order of the approximate dynamic system is determined by the zero-order holder. The state and the ISWEC system are discretized according to the sampling time. In order to simplify the above equation, the time variable k represents the overall sampling time; that is, $k = lT_s, l \in N$. The above cost function and the discrete time state space equation can be expressed in the following forms:

$$\min_M J(k) = \sum_{i=0}^{N_p-1} x^T(k+i|k)PM(k+i|k) + \sum_{i=0}^{N_c-1} M^T(k+i|k)RM(k+i|k)$$

$$\dot{x}_2(k) = -a_1\dot{\delta}(k) - a_3\dot{\delta}^3(k) - b_1\delta(k) - b_3\delta^3(k) - b_5\delta^5(k) + \frac{M_D h_{GM}\alpha(k)}{I_\delta + \Delta I_\delta} - \frac{2nh_0\varepsilon(k)\cos\dot{\varepsilon}(k)}{I_\delta + \Delta I_\delta},$$

$$\dot{x}_4(k) = \frac{h_0\dot{\delta}\cos\varepsilon(k)}{J} - \frac{M(k)}{J} - \frac{x_{offset}M_G\sin\varepsilon(k)}{J}, \tag{22}$$

s.t
$$|M(k+i|k)| \le M_{max}, \quad i = 0,\ldots,N_c-1,$$
$$|\varepsilon(k+i|k)| \le \varepsilon_{max}, \quad i = 0,\ldots,N_p-1,$$
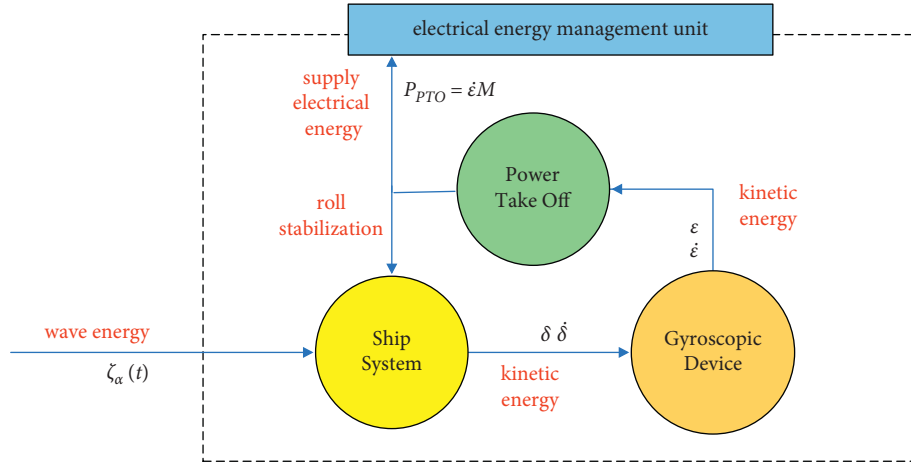$$|\dot{\varepsilon}(k+i|k)| \le \dot{\varepsilon}_{max}, \quad i = 0,\ldots,N_p-1,$$

FIGURE 2: The relationship of energy transfer and conversion in ISWEC system.

where $N_p \in N$ is the prediction range and $x(k+i|k)$ represents the motion prediction of the system state.

4. Results and Discussions

4.1. Parameter Setting. In the simulation experiment, taking the ship parameters of a fishery administration ship as an example [41], the optimization effect of different approaches on ISWEC power generation is investigated. The basic parameters of the ship as well as the gyroscopic system are shown in Table 1.

In the simulation parameters configuration, set the harmonic frequency step $\Delta\omega = 0.1$ rad/s, the integration time step $T_s = 0.02$ s, the simulation time is 200s, and the heading angle is $\psi = 90°$. The total mass of the designed gyroscopic rotor and the frame is 2800 kg , the inertia moment of the flywheel around Oz is $I = 229.7$ kg·m^2, the moment of inertia around the precession axis Oy is $J = 25$ kg·m^2, and the rotating speed of the flywheel is $w_0 = 3000$ r/min. One pair of gyros is employed to generate power. Because the motor is amounted in the lower part of the gyroscope device, the gravity center of the gyroscope moves down $x_{offset} = 12.5$ mm. The initial conditions are configured as follows: $\delta = 0, \dot{\delta} = 0, \varepsilon = 0, \dot{\varepsilon} = 0$.

In MPC method, when the prediction range is set too long, the computational burden of the nonlinear solver can be increased, and when the prediction range is set too short, the MPC method may lose the prediction ability about the system. During the experimental simulation, it can be found that when the prediction range is greater than or equal to 4, the energy conversion efficiency of ISWEC cannot be improved significantly. In addition, the calculation speed can meet the real-time requirements, so the value of the prediction range is 4.

The state feedback controller of LQR method is uniquely determined by the weight matrices Q, N, and r_T, so the value of Q, N, and r_T should be set properly. Improper weight coefficient may lead to the decrease of the control accuracy or even the system instability. In the simulation experiment, the optimal Q, N, and r_T matrices are obtained after a lot of repeated testing [18]. The parameters of the controllers are

TABLE 1: The parameters of the coupled system.

Quantity	Value
Ship length L	30.70 m
Ship width b	6.90 m
Ship depth h	4.96 m
Ship draft Z	2.67 m
Displacement M_D	195 t
Transverse metacentric height h_{GM}	0.962 m
Damping coefficient a_1	0.0208
Damping coefficient a_3	0.0165
Restoring moment coefficient b_1	2.032
Restoring moment coefficient b_3	−0.743
Restoring moment coefficient b_5	0.0643
Total moment of inertia $(I_\delta + \Delta I_\delta)$	1078 (t·m^2)
Initial natural frequency of roll ω_0	1.32 (rad·s^{-1})

set as follows: $Q = \text{diag}[0, 0, 2 \times 10^7, 0]$, $N = [0, 0, 0, -0.8]$, and $r_T = 1$ in the LQR method, while, in the NMPC approach, $P = [0, 0, 0, -40]$, $R = 0$, the prediction range is $N_p = 4$, the control range is $N_c = 4$, the precession angle range is $\pm 70°$, and the precession angular velocity range is ± 8rad/s.

It should be noted that although both LQR and MPC methods obtain the optimal control solution of cost function, their working principles are different, resulting in different cost function description and parameters in the face of the same control index. Structurally, LQR controller cannot get the optimization solution within constraints; hence, the precession angular velocity should be limited in the cost function, which is a soft constraint. In MPC, the precession angular velocity can be listed in the constraint expression, which is a hard constraint. The different working principles of the two control methods make their cost functions different. The soft constraint and hard constraint on the control torque exist simultaneously in MPC, but the hard constraint should be satisfied in any case. Under the normal power generation situation, the torque control can be completely limited by the hard constraint. Therefore, the weight coefficient corresponding to the control torque in the cost function can be set to zero. When the unmanned ship
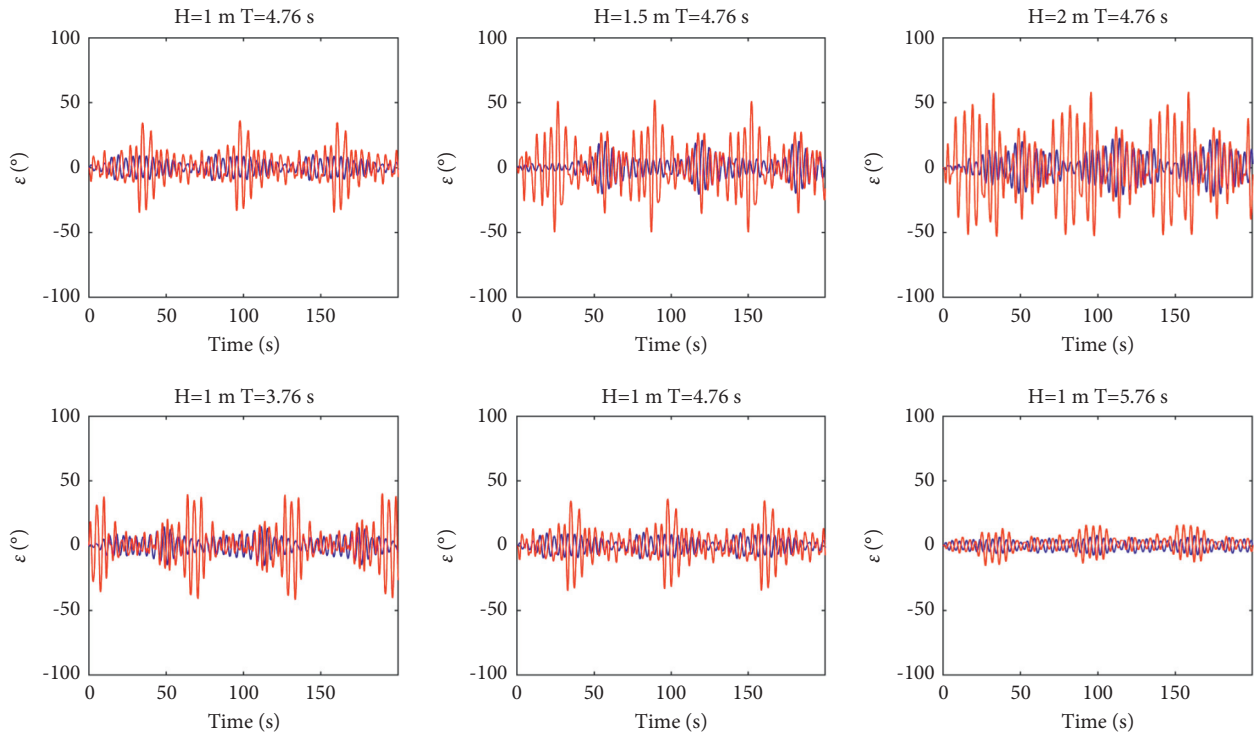
FIGURE 3: The precession angle response comparison of the gyroscopic system under the random wave circumstance using LQR and NMPC, respectively. The red curve represents the NMPC controller, and the blue curve represents the LQR controller.
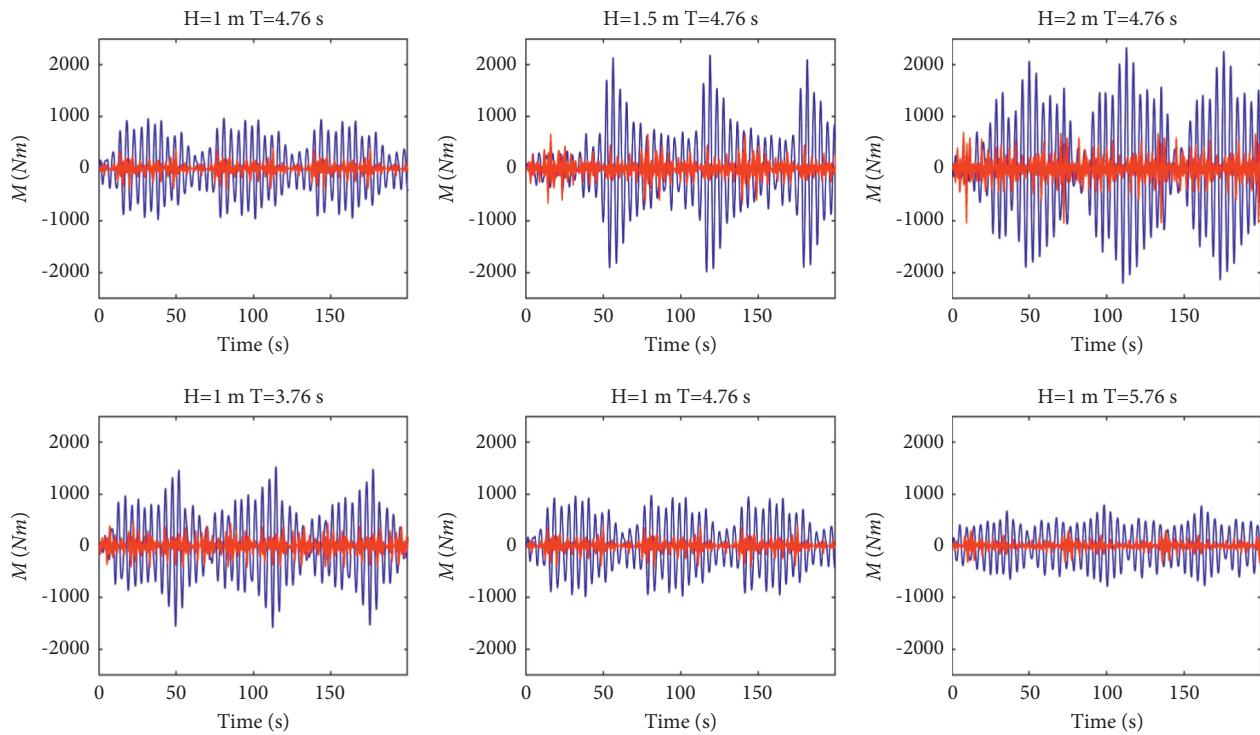

FIGURE 4: The control torque comparison of the gyroscopic system under the random wave circumstance using LQR and NMPC, respectively. The red curve represents the NMPC controller, and the blue curve represents the LQR controller.
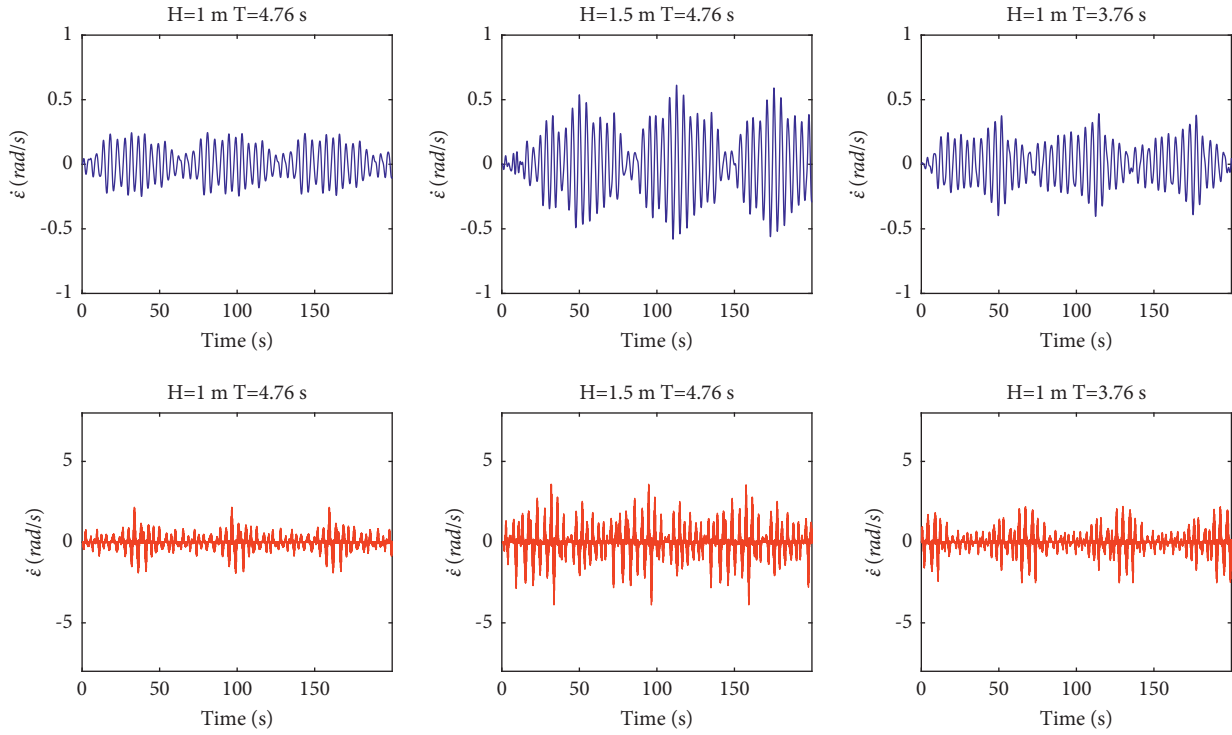
FIGURE 5: The precession angular velocity response comparison of the gyroscopic system under the random wave circumstance using LQR and NMPC, respectively. The red curve represents the NMPC controller, and the blue curve represents the LQR controller.
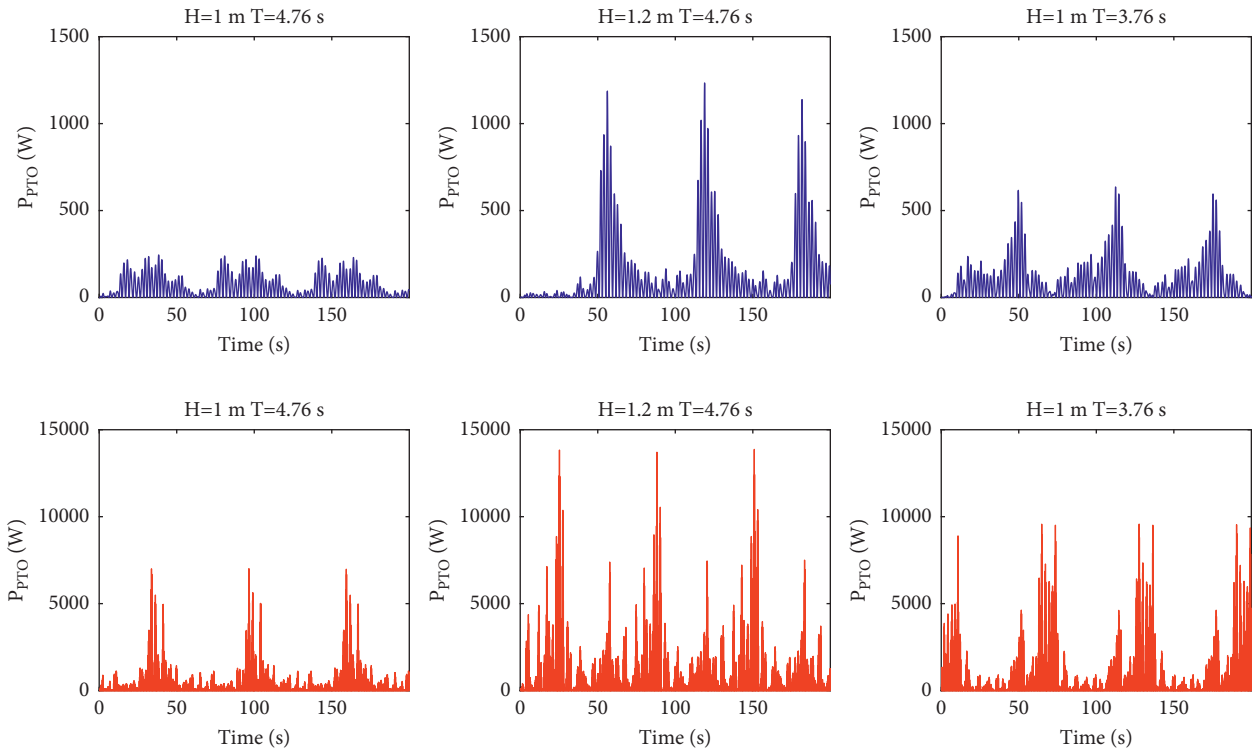

FIGURE 6: The power generation performance comparison of the gyroscopic system under the random wave circumstance using LQR and NMPC, respectively. The red curve represents the NMPC controller, and the blue curve represents the LQR controller.

exists without the wind and waves, the generated power is not enough to compensate for the power consumption of the controller. At this time, the weight coefficient will be set to a large value, and the system stays still.

4.2. Simulation Results and Analysis. Figures 3–6 show the comparison results of the precession angle, the precession speed, the control torque, and the average power under NMPC and LQR controllers, respectively. Figure 3 indicates the response of the gyroscopic precession angle when height and period of the random wave vary. It can be noted that the change trend of NMPC precession angle is similar to LQR when the input signal is the same, but the change range is larger than that of LQR controller. However, considering that MPC method limits the range of gyro precession angle, the maximum precession angle of NMPC cannot exceed the limit of ISWEC device. Thus, the gyro system can still remain in normal operation.

As is described in Figure 4, the control torque is adjusted according to the changes of the wave height and period parameters of the random wave. By observing the system response performance of two different control systems, it can be drawn that, under a variety of different random wave excitations, the NMPC method can adjust the control damping in a smaller state range, thereby ensuring that the energy cost is smaller.

As is seen in Figure 5, ISWEC gyro precession angular velocity varies when the height and the period of the random wave alter. It can be demonstrated that when the autonomous ship sails in different situations, the gyro precession angular velocity response of NMPC controller varies in a larger range compared with LQR. The air resistance to precession dissipates part of the energy. However, since the precession speed of the gyroscope is far less than the speed of the flywheel, the energy dissipation caused by precession motion can be ignored when compared with the energy consumed by the flywheel motor.

Figure 6 describes the change of the power generated by ISWEC when the height and period of the random wave vary. Under the same wave input conditions, the peak of the energy power generated by NMPC via converting wave energy is much larger than that of LQR controller, which shows that NMPC method has more potential to exploit the ocean energy. However, more attention should be devoted to the selection of the maximum power parameters of the PTO generator to ensure the normal operation of the power generation system.

In order to compare the performances of the MPC method and the LQR approach in terms of power generation, quantitative analysis can be conducted by recording power optimization percentage. Table 2 shows the average power and power optimization percentage of MPC and LQR when exposed to different wave excitation, where P_r is power optimization percentage of NMPC relative to LQR. The expression for P_r is as follows:

TABLE 2: The energy output performance comparison of the inertial gyroscopic power generation system using LQR and NMPC.

| Wave form	ID	$T(s)$	$H(m)$	$P_{LQR}(W)$	$P_{NMPC}(W)$	$P_r(\%)$
Regular wave	1	6.67	1	343.3792	618.2858	80.1
Regular wave	2	6.67	1.2	452.4887	707.8485	56.4
Regular wave	3	6.67	1.5	673.0425	822.4701	22.2
Regular wave	4	6.47	1	412.6509	708.1611	71.6
Regular wave	5	6.87	1	287.9671	543.5923	88.7
Random wave	1	4.76	1	56.2079	73.8244	31.3
Random wave	2	4.76	1.5	125.3348	171.6652	40.0
Random wave	3	4.76	2	224.8610	305.8372	36.0
Random wave	4	3.76	1	90.4005	128.0555	41.7
Random wave	5	5.76	1	31.1759	42.1092	35.1
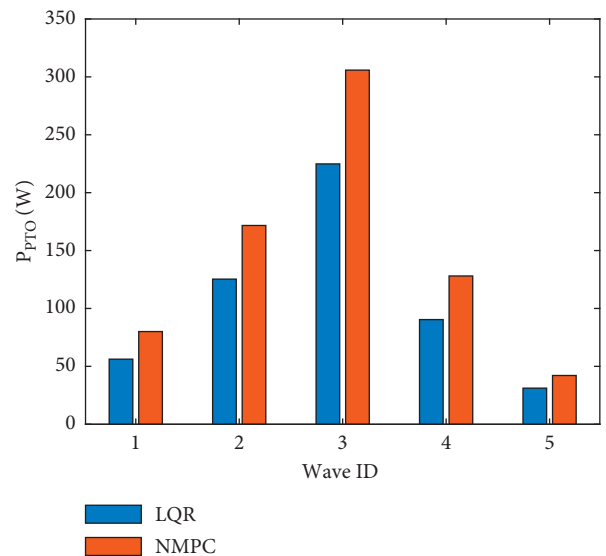
FIGURE 7: The power comparison of LQR and NMPC when exposed to the random wave environment.

$$P_r = \frac{P_{NMPC} - P_{LQR}}{P_{LQR}} \times 100\%. \tag{23}$$

The change of ISWEC power generation is indicated in Figure 7 when the significant wave height and average wave period of random waves vary. Under different wave heights and average wave periods, the electric power converted by the MPC method based on the nonlinear model is better than the power generated by the LQR method. In addition, under the condition of random wave stimulation, the power generation of ISWEC is only related to the significant wave height and the average wave period. It can be obtained that as the significant wave height gets larger and the average wave period becomes smaller, the power generation of the ISWEC system can be enhanced.

As is shown in Figure 8, ISWEC power generation varies when the regular wave height and period parameters alter. Similar to the random waves, the power generation efficiency of the NMPC method outperforms the LQR.
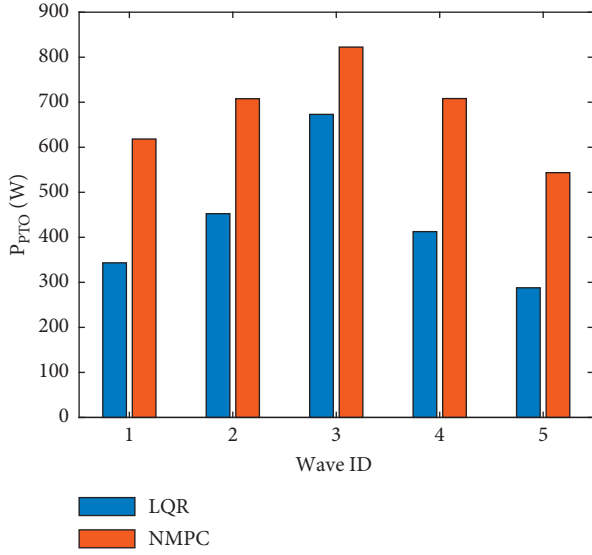
FIGURE 8: The power comparison of LQR and NMPC when exposed to the regular wave environment.
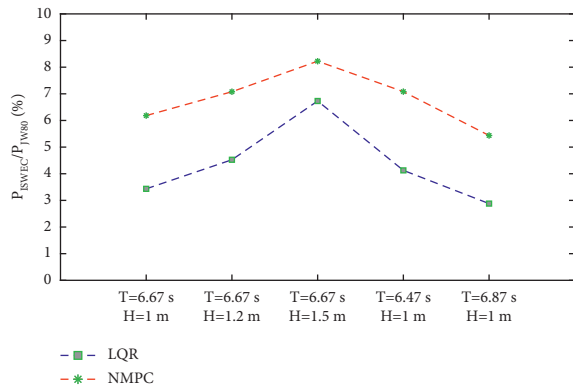

FIGURE 9: The compared power compensation ratio by LQR method and NMPC method, respectively.

Moreover, since the period of the regular wave is constant, it is easier to resonate with the natural frequency of the ship hull. Comprehensively, the overall power generation efficiency under regular waves circumstance is preferable to the one obtained from the random waves.

The energy consumed by the flywheel motor is mainly used to drive the rotor to rotate at high speed, so the energy consumed is mainly related to the angular velocity of the flywheel and the inertia torque of the gyro rotor. The angular momentum of JW-80 (10 kW) gyro rotor from Shanghai Jiwu Technology Co., Ltd. is similar to the angular momentum designed in the experiment. $P_{JW80}^{ISWEC} = (P_{ISWEC}/P_{JW80}) \times 100\%$ is used to represent the compensation effect of ISWEC on JW-80 power system, and the gyro generator can compensate about $3\% - 8\%$ of the power system energy consumption. The compared power compensation ratio by LQR method and NMPC method is given in Figure 9.

Due to higher power generation efficiency of NMPC, the compensation effect for the ship power system is better than

that of LQR controller, as listed in Figure 9. Furthermore, when the wave period gets longer and the wave height becomes smaller, there is an increasing power discrepancy between NMPC and LQR. Thus, it can be drawn that, under different types of wave excitation, NMPC method outperforms LQR approach in improving power generation efficiency.

5. Conclusions

In this paper, a simultaneous dynamic model of the power take-off power generation system, the gyroscopic device, and the ship nonlinear model in roll channel is established, and a nonlinear model predictive control method is introduced to improve the power generation efficiency of the gyroscopic device. The presented control method can achieve online optimization with the help of an efficient nonlinear solver. The objective function and its constraint conditions are determined through comprehensively considering the power output torque, precession angle, and precession angular velocity saturation in the real system. The proposed control method is adopted for the control simulation of the linear and nonlinear dynamic models. The results prove that the control method based on the nonlinear model has higher power generation efficiency than the linear control method when exposed to different types of waves excitation. It is of certain significance to optimize and improve the energy storage structure of unmanned ships in the future.

Abbreviations

NMPC: Nonlinear model predictive control
ISWEC: Inertial sea wave energy converter
WEC: Wave energy converter
PTO: Power take-off
USV: Unmanned Surface Vehicle
LQR: Linear quadratic regulator.

Data Availability

Part of the ship parameters are from Shanghai Jiwu Technology Co., Ltd., Shanghai, China, and part of the wave data are referred to the public data of the State Oceanic Administration of China.

Conflicts of Interest

The authors declare no conflicts of interest.

Authors' Contributions

Nailong Wu and Shaonan Chen conceptualized the study; Nailong Wu and Xinyuan Chen were responsible for methodology and investigated the data; Xinyuan Chen was responsible for software, performed data curation, and visualized the study; Xinyuan Chen, Nailong Wu, and Haodong Yuan validated the data and prepared the original draft; Xinyuan Chen, Jie Qi, and Nailong Wu performed formal analysis; Shaonan Chen was responsible for resources; Nailong Wu and Haodong Yuan reviewed and

References

[1] T. I. Fossen, *Guidance and Control of Ocean Vehicles*, John Wiley & Sons Inc, Chichester, England, 1994.

[2] G. S. Lima, S. Trimpe, and W. M. Bessa, "Sliding mode control with gaussian process regression for underwater robots," *Journal of Intelligent & Robotic Systems*, vol. 99, no. 3-4, pp. 487–498, 2020.

[3] Y. Wang, X. Xie, M. Chadli, S. Xie, and Y. Peng, "Sliding mode control of fuzzy singularly perturbed descriptor systems," *IEEE Transactions on Fuzzy Systems*, vol. 29, 2020.

[4] N. L. Wu, X. Y. Wang, T. Ge, C. Wu, and R. Yang, "Parametric identification and structure searching for underwater vehicle model using symbolic regression," *Journal of Marine Science and Technology*, vol. 22, no. 1, pp. 51–60, 2017.

[5] L. Yu, Q. Meng, and H. Zhang, "3-dimensional modeling and attitude control of multi-joint autonomous underwater vehicles," *Journal of Marine Science and Engineering*, vol. 9, no. 3, p. 307, 2021.

[6] D. Ji, Z. Deng, S. Li et al., "A novel case of practical exponential observer using extended kalman filter," *IEEE Access*, vol. 6, pp. 58004–58011, 2018.

[7] W. Zhou, Y. Wang, C. K. Ahn, J. Cheng, and C. Chen, "Adaptive fuzzy backstepping-based formation control of unmanned surface vehicles with unknown model nonlinearity and actuator saturation," *IEEE Transactions on Vehicular Technology*, vol. 69, no. 12, pp. 14749–14764, 2020.

[8] T. Aderinto and H. Li, "Ocean wave energy converters: status and challenges," *Energies*, vol. 11, no. 5, p. 1250, 2018.

[9] D. Vicinanza and P. Contestabile, *Renewable Energy from the Oceans: From Wave, Tidal and Gradient Systems to Offshore Wind and Solar*, The Institution of Engineering and Technology (IET) Digital Library, London, UK, 2019.

[10] D. Magagna and A. Uihlein, "Ocean energy development in Europe: current status and future perspectives," *International Journal of Marine Energy*, vol. 11, pp. 84–104, 2015.

[11] G. Bracco, E. Giorcelli, G. Mattiazzo, M. Pastorelli, and M. Raffero, "Control of an ISWEC wave energy harvest system," *IEICE Proceedings Series*, vol. 2, pp. 166–169, 2013.

[12] G. Bracco, E. Giorcelli, G. Mattiazzo, V. Orlando, and M. Raffero, "Hardware-in-the-loop test rig for the ISWEC wave energy system," *Mechatronics*, vol. 25, pp. 11–17, 2015.

[13] G. Bracco, E. Giorcelli, G. Mattiazzo, M. Pastorelli, and J. Taylor, "ISWEC: design of a prototype model with gyroscope," in *Proceedings of the 2009 International Conference on Clean Electrical Power*, pp. 57–63, IEEE, Capri, Italy, June 2009.

[14] G. Bracco, E. Giorcelli, and G. Mattiazzo, "ISWEC: a gyroscopic mechanism for wave power exploitation," *Mechanism and Machine Theory*, vol. 46, no. 10, pp. 1411–1424, 2011.

[15] M. Raffero, M. Martini, B. Passione, G. Mattiazzo, E. Giorcelli, and G. Bracco, "Stochastic control of inertial sea wave energy converter," *The Scientific World Journal*, vol. 2015, Article ID 980613, 14 pages, 2015.

[16] G. Vissio, D. Valério, G. Bracco, P. Beirão, N. Pozzi, and G. Mattiazzo, "ISWEC linear quadratic regulator oscillating control," *Renewable Energy*, vol. 103, pp. 372–382, 2017.

[17] G. Bracco, E. Giorcelli, G. Mattiazzo et al., "Application of linear model predictive control to the ISWEC," in *Proceedings of the Renewable Energies Offshore—1st International Conference on Renewable Energies*, pp. 257–264, Lisbon, Portugal, September 2015.

[18] G. Bracco, M. Canale, and V. Cerone, "Optimizing energy production of an inertial sea wave energy converter via model predictive control," *Control Engineering Practice*, vol. 96, Article ID 104299, 2020.

[19] G. Bracco, M. Canale, and V. Cerone, "Energy harvesting optimization of an inertial sea wave energy converter through model predictive control," in *Proceedings of the 2019 IEEE 15th International Conference on Control and Automation (ICCA)*, pp. 85–90, IEEE, Edinburgh, UK, July 2019.

[20] M. Richter, M. E. Magana, O. Sawodny, and T. K. Brekken, "Nonlinear model predictive control of a point absorber wave energy converter," *IEEE Transactions on Sustainable Energy*, vol. 4, no. 1, pp. 118–126, 2012.

[21] A. Mérigaud and J. V. Ringwood, "Towards realistic nonlinear receding-horizon spectral control of wave energy converters," *Control Engineering Practice*, vol. 81, pp. 145–161, 2018.

[22] W. E. Cummins, "The impulse response function and ship motions," *Schiffstechnik*, vol. 9, pp. 101–109, 1962.

[23] D. Chiccoli, "Design and control of a hydraulic power take-off for the ISWEC," Doctoral dissertation, Politecnico di Torino, Turin, Itlay, 2018.

[24] G. Bracco, A. Cagninei, E. Giorcelli, G. Mattiazzo, D. Poggi, and M. Raffero, "Experimental validation of the ISWEC wave to PTO model," *Ocean Engineering*, vol. 120, pp. 40–51, 2016.

[25] J. V. Ringwood, G. Bracco, and F. Fusco, "Energy-maximizing control of wave-energy converters: the development of control system technology to optimize their operation," *IEEE Control Systems Magazine*, vol. 34, no. 5, pp. 30–55, 2014.

[26] L. Chisci, J. A. Rossiter, and G. Zappa, "Systems with persistent disturbances: predictive control with restricted constraints," *Automatica*, vol. 37, no. 7, pp. 1019–1028, 2001.

[27] S. K. Kommuri, M. Defoort, H. R. Karimi, and K. C. Veluvolu, "A robust observer-based sensor fault-tolerant control for PMSM in electric vehicles," *IEEE Transactions on Industrial Electronics*, vol. 63, no. 12, pp. 7671–7681, 2016.

[28] S. K. Yang, "Observer-based anti-windup compensator design for saturated control systems using an LMI approach," *Computers & Mathematics with Applications*, vol. 64, no. 5, pp. 747–758, 2012.

[29] N. Wang and H. R. Karimi, "Successive waypoints tracking of an underactuated surface vehicle," *IEEE Transactions on Industrial Informatics*, vol. 16, no. 2, pp. 898–908, 2019.

[30] N. Wu, M. Wang, T. Ge, C. Wu, D. Yang, and R. Yang, "Experiments on high-performance maneuvers control for a work-class 3000-m remote operated vehicle," *Proceedings of the Institution of Mechanical Engineers, Part I: Journal of Systems and Control Engineering*, vol. 233, no. 5, pp. 558–569, 2019.

[31] B. D. Anderson and J. B. Moore, *Optimal Control: Linear Quadratic Methods*, Courier Corporation, Dover Publications Inc., Mineola, NY, USA, 2007.

[32] S. Zhan, G. Li, J. Na, and W. He, "Feedback noncausal model predictive control of wave energy converters," *Control Engineering Practice*, vol. 85, pp. 110–120, 2019.

[33] X. Mi, Y. Zou, S. Li, and H. R. Karimi, "Self-triggered DMPC design for cooperative multiagent systems," *IEEE Transactions on Industrial Electronics*, vol. 67, no. 1, pp. 512–520, 2019.

[34] M. Yuan, Z. Chen, B. Yao, and X. Liu, "Fast and accurate motion tracking of a linear motor system under kinematic and dynamic constraints: an integrated planning and control approach," *IEEE Transactions on Control Systems Technology*, vol. 29, 2019.

[35] N. Faedo, S. Olaya, and J. V. Ringwood, "Optimal control, MPC and MPC-like algorithms for wave energy systems: an overview," *IFAC Journal of Systems and Control*, vol. 1, pp. 37–56, 2017.

[36] Y. Wang and S. Boyd, "Fast model predictive control using online optimization," *IEEE Transactions on Control Systems Technology*, vol. 18, no. 2, pp. 267–278, 2009.

[37] J. Luna, O. Falkenberg, S. Gros, and A. Schild, "Wind turbine fatigue reduction based on economic-tracking NMPC with direct ANN fatigue estimation," *Renewable Energy*, vol. 147, pp. 1632–1641, 2020.

[38] S. Kolluri, S. V. Aduru, M. Pathak, R. D. Braatz, and V. R. Subramanian, "Real-time nonlinear model predictive control (NMPC) strategies using physics-based models for advanced lithium-ion battery management system (BMS)," *Journal of the Electrochemical Society*, vol. 167, no. 6, Article ID 063505, 2020.

[39] Q. Zheng, Z. Xu, H. Zhang, and Z. Zhu, "A turboshaft engine NMPC scheme for helicopter autorotation recovery maneuver," *Aerospace Science and Technology*, vol. 76, pp. 421–432, 2018.

[40] J. A. E. Andersson, J. Gillis, G. Horn, J. B. Rawlings, and M. Diehl, "CasADi: a software framework for nonlinear optimization and optimal control," *Mathematical Programming Computation*, vol. 11, no. 1, pp. 1–36, 2019.

[41] Z. Wu, Li. Yang, S. Chen, and Y. Huang, "Hydraulic damping gyro anti rolling device for ship nonlinear rolling," *Mechanical Design and Research*, vol. 32, no. 2, pp. 65–68, 2016.

[42] D. Ning, H. Du, N. Zhang, S. Sun, and W. Li, "Controllable electrically interconnected suspension system for improving vehicle vibration performance," *IEEE/ASME Transactions on Mechatronics*, vol. 25, no. 2, pp. 859–871, 2020.

[43] J. Lu and S. Chen, "Active gyro-stabilizer for nonlinear roll suppression of marine vehicles," *Journal of Mechanical Engineering*, vol. 47, no. 19, pp. 86–90, 2011.

[44] W. Froude, *On the Rolling of Ships*, Transactions, Read at the Second Session of the Institute of Naval Architects, 1862, http://resolver.tudelft.nl/uuid:f2ca1095-6245-41fb-8b02-4c6f3bb50364.

[45] M. R. Haddara and X. Wu, "Parameter identification of nonlinear rolling motion in random seas," *International Shipbuilding Progress*, vol. 40, no. 423, pp. 247–260, 1993.

[46] M. R. Haddara and P. Bennett, "A study of the angle dependence of roll damping moment," *Ocean Engineering*, vol. 16, no. 4, pp. 411–427, 1989.